Chapter 7

Microstructure-Tailored Stainless Steels with High Mechanical Performance at Elevated Temperature

Kamran Saeidi and Farid Akhtar

Additional information is available at the end of the chapter

http://dx.doi.org/10.5772/intechopen.80468

Abstract

Stainless steels are widely used in chemical, structural and automotive applications due to their high room-temperature mechanical properties, toughness, corrosion resistance and low cost. However, tendency and rise in industrial demands for components to be used at high temperature with good mechanical performance and corrosion resistance limit their usage in many applications and narrow down their service criteria. Tailoring the microstructure, tuning the chemistry, adjusting the phase composition and introducing a dense 3D network of dislocations can tailor and develop stainless steels with high performance for extreme conditions, such as elevated temperatures. In this chapter, the effect of the microstructure of additively manufactured and thermo-mechanically processed stainless steels on the high temperature mechanical performance is discussed and a comparison is made with conventional steels. Moreover, new mechanisms are introduced and discussed co-relating the microstructure and properties.

Keywords: stainless steel, selective laser melting, microstructure tailoring, high temperature, mechanical properties

1. Introduction

Additive manufacturing (AM) has been developed from prototyping to near net shape and end products which can challenge and compete with the traditional manufacturing methods such as casting, pressing and sintering. The components of materials, such as stainless steel, are built up with unique structures at various length scales spanning from macro down to nano metric levels which are different from materials produced by conventional methods. The AM technique makes it possible to assemble localized tuneable structures, tailor the chemistry and microstructure and advance the mechanical, physical and corrosion properties

to produce customized materials. The tailoring and manipulation of the materials chemistry and the microstructure not only improves the room temperature mechanical properties of stainless steels but provides opportunities to design stainless steels for elevated temperatures and for relatively harsh environments. Industrial demands show that the stainless steels are of interest for high temperature applications nowadays since these materials can compete in price with other materials and therefore be more efficient and economical. This chapter introduces AM manufactured stainless steels (316L, 2507 and 420) and their post processing to tailor microstructures to achieve advanced mechanical properties both at room temperature and elevated temperatures and make comparisons with traditionally manufactured stainless steels. The outcome of this work is undoubtedly of interest for engineers and scientists.

2. Additive manufacturing

Additive manufacturing is a flexible technique that can manufacture three-dimensional (3D) solid objects of virtually any geometry from digital design data based on computer aided design and computer aided manufacturing (CAD/CAM). The AM technique builds up objects in a bottom-up approach, i.e. by adding material layer by layer on top of each other and consolidating it using a high energy heating source [1]. Early use of AM in the form of rapid prototyping focused on pre-production and nowadays AM is being used to fabricate end-use products. AM can be used to process materials such as plastics, polymers, metals, alloys, ceramics and human tissue. Based on the raw materials used, AM is categorized into three main groups: (I) solid-based, such as laminated object manufacturing (LOM) [2] where cut to shape laminates are bonded together; (II) liquid-based, such as fused deposition modeling (FDM) [3] Stereo-lithography (SLA) where a photosensitive polymer resin is cured layer by layer using a scanning ultraviolet laser beam [4, 5]; and (III) powder-based, such as selective laser sintering (SLS) or selective laser melting (SLM) [6–8] where layers are created by spreading the powder on the building substrate and melting the powder particles bonding them together using a high energy laser source (see **Figure 1**), and electron beam source, i.e., electron beam melting (EBM) [9–11] and three-dimensional printing (3DP) [12, 13] where layers are created from powders onto which a traversing ink jet head prints a bonding agent. LOM, FDM, SLA and 3DP can produce metal parts in an "indirect" approach in which a binder is used to bond precursor particles forming 3D parts and post-processing is required after the AM process. SLS/SLM, EBM are "direct" ways in which the precursor particles are partially melted and/or fully melted during the AM process to make the final part directly. In the following sections, the SLM processing of stainless steels and post processing to tailor structure and properties are discussed.

SLM is used to fabricate metallic prototypes, components and counterparts in various industrial applications such as aerospace, defense, spacecraft, automobile and the biomedical industries. **Figure 2** shows examples of products built by SLM technology.

For SLM fabrication of materials two requirements have to be met:

- **Powder precursor:** the powder should be provided as gas atomized spherical granules with size between 25 and 150 μm. The powder should have a good flowability to ensure

http://dx.doi.org/10.5772/intechopen.80468

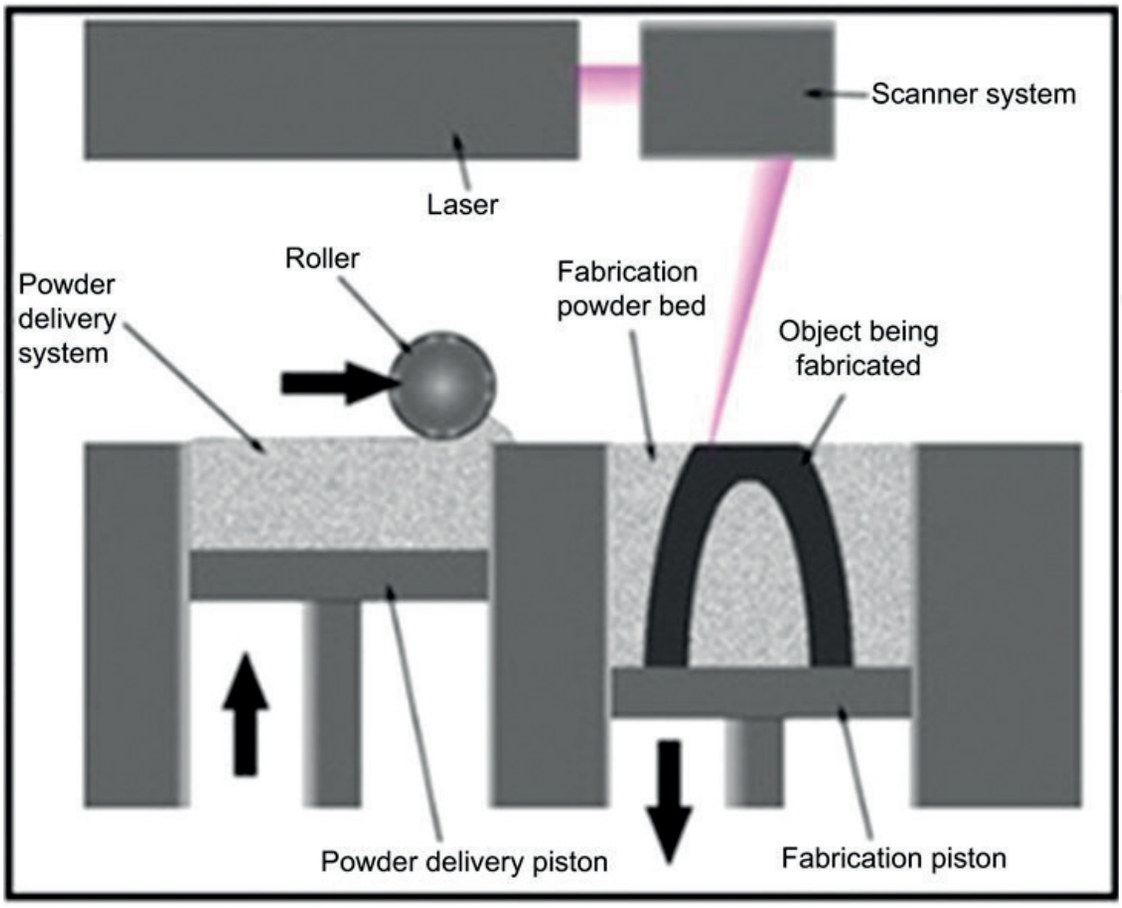

Figure 1. Schematic of the selective laser melting process (http://blog.trendonix.com/3d-printing-selective-laser-sintering).

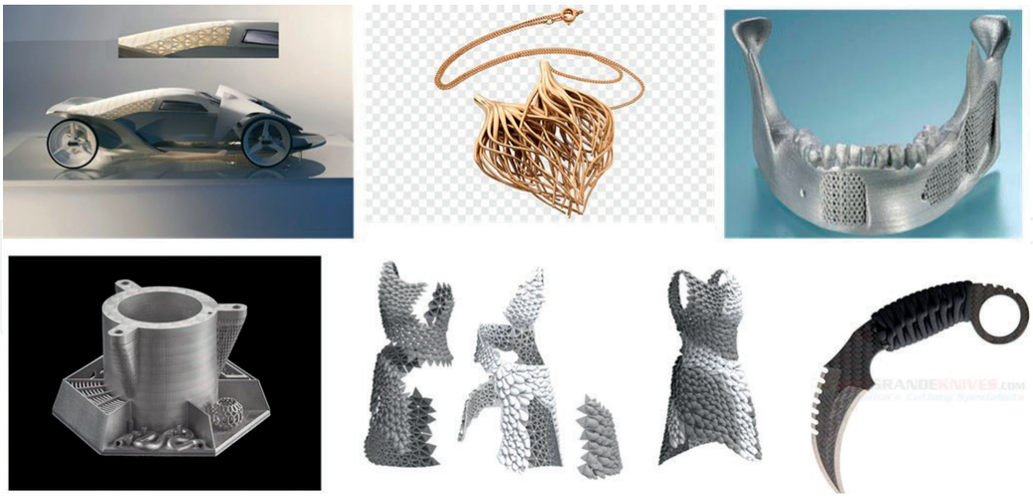

Figure 2. Example of products in different application fields produced by SLM technology (courtesy of Saeidi [14]).

unified spreading of the powder by the re-coater blade on the building substrate and an acceptable apparent density to avoid sinking of the powder.

- **Optimization of the processing parameters:** laser processing parameters are optimized to ensure a solid and decent part. The main parameters are laser power (P), scan speed (v),

focal spot diameter (2a), line spacing (L) and layer thickness (t). Because of strong association between the laser power and scan speed a suitable way of expressing their influences on powder interaction is in the form of a compound variable (Eq.1) which is referred to as the laser energy density (LED) [1].

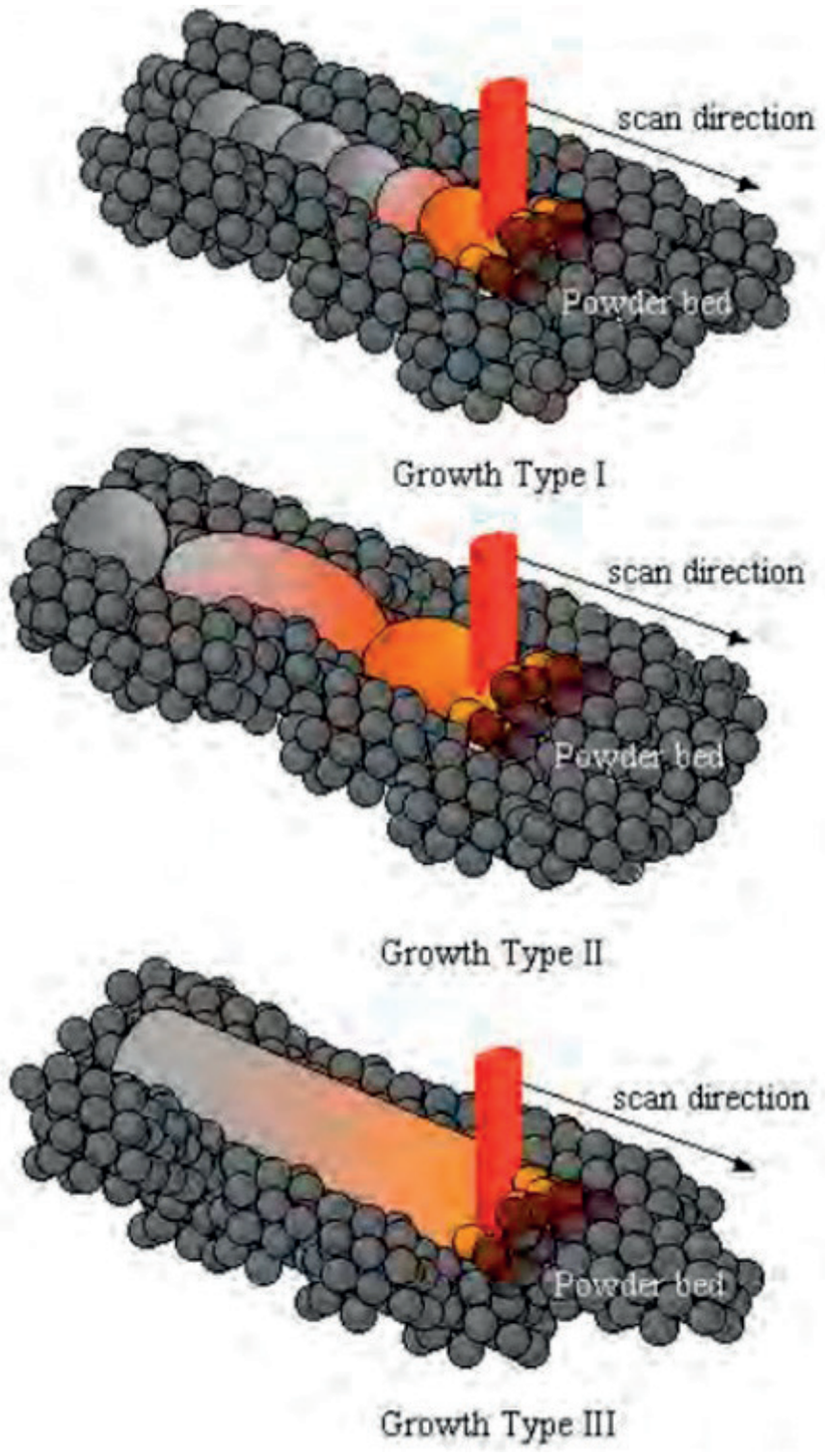

Figure 3. Three types of melt pools with growth type I (balled melt pool) type II (discontinuous and fragmented melt pools) and type III (continuous melt pool columns) (courtesy of Beng [15]).

http://dx.doi.org/10.5772/intechopen.80468

$$LED = P/2a.V \quad (1)$$

During SLM, upon exposure of powder with the laser beam momentarily melt droplets are created and due to the moving beam elongated melt pools are created. These melt pools can be regarded as small casting. The shape of the melt pools can be controlled by the surface tension of the melt. The solidification of the melt results in the formation of microstructure within the melt pools, thus the shape and size of the melt pool are controlled and adjusted [15]. The size and shape of melt pools can be adjusted by controlling the laser processing parameters. Three different melt pool types, (I) balled melt pools; (II) discontinuous and fragmented melt pools; and (III) continuous melt pools have been identified in laser processing of materials, as shown in **Figure 3**. The fast cooling rate (10^5 KS^{-1}) for metallic materials and the confined melt pool results in unique microstructures [14].

2.1. Fabrication of stainless steels using SLM

Stainless steels are one of the most widely investigated materials for SLM [16] and based on the laser processing parameters and LED discussed above, SLM can fabricate dense [17, 18] and porous stainless steels used in aerospace, automotive, fuel cells [19] and biomedical applications [20, 21]. In this chapter, fabrication of stainless steel grades such as austenitic 316L, duplex 2507 and martensitic 420 grades with SLM technique and post processing of the stainless steels will be discussed and their influence on the microstructure and mechanical properties will be explained.

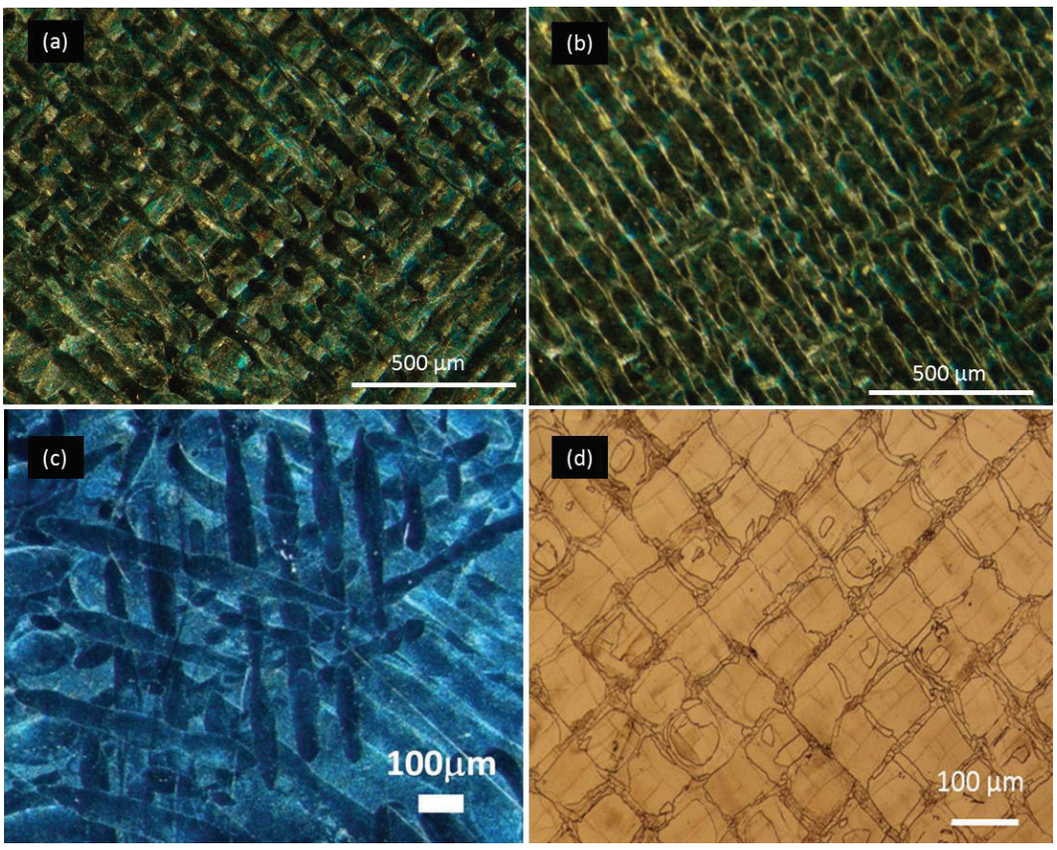

Figure 4. Different melt pool patterns caused by different scanning strategies during SLM of (a and b) 316L austenitic stainless steel, (c) CrCoMo dental alloy, (d) 2507 duplex stainless steel (figures have not been published elsewhere).

2.2. Microstructure hierarchies and heterogeneities in SLM stainless steel components

Hierarchical assembly of materials is one of the most promising yet challenging aspects of nanoscience [22–24]. Although synthesizing hierarchical materials, in terms of complexity and precision, is still very primitive, advanced progress has already been made towards this field. Recently, hierarchical structures are processed in materials, e.g., Ni-base super alloys processed by rapid solidification of the melt [25, 26]. Hierarchies in laser induced coating of Ti6Al4V alloys, in which a multi-scale textured zirconia coating was applied on titanium alloy using a pulsed laser, has been reported [27]. Lui et al. [28] synthesized W-Cr alloys with hierarchical structure using combustion synthesis. However, hierarchies in stainless steel have been reported recently [18] in the microstructure of selective laser melted steels. During SLM

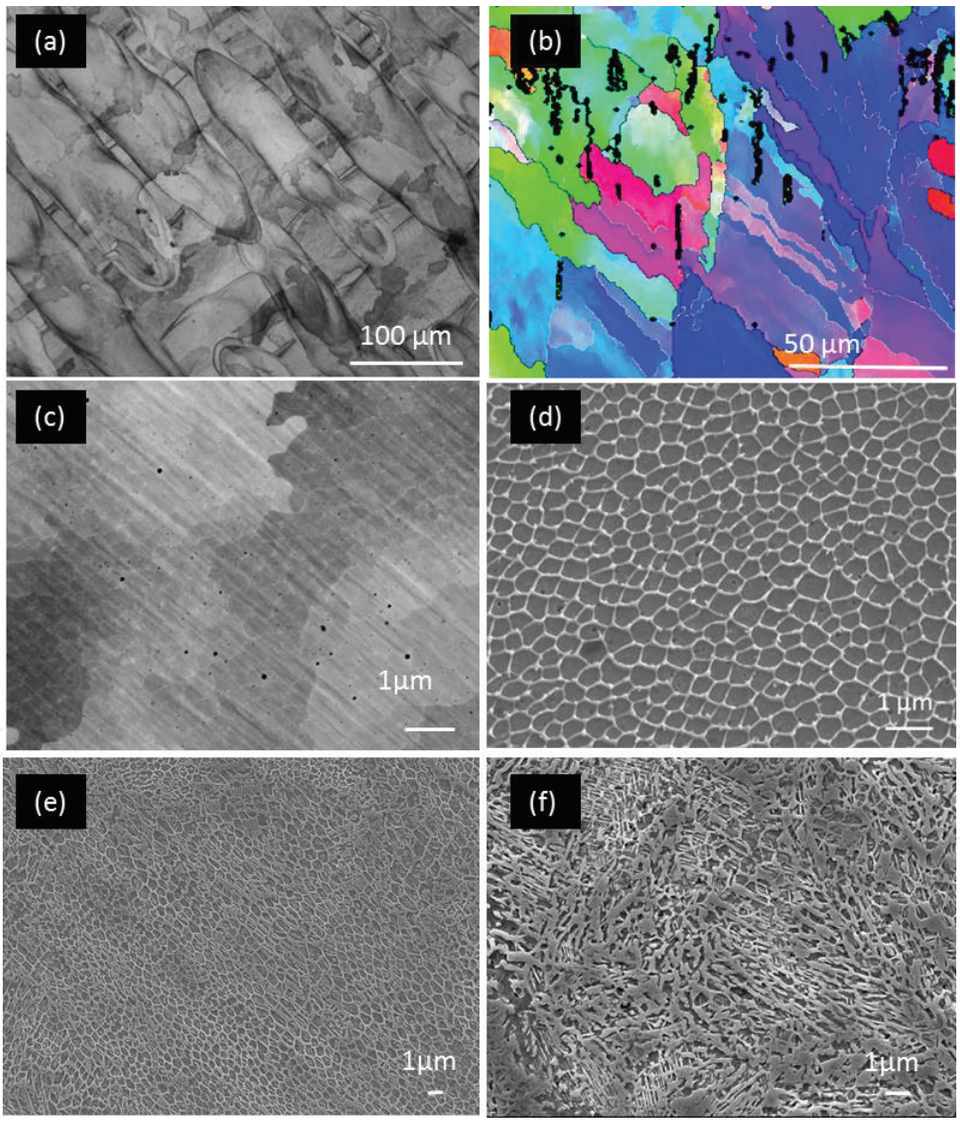

Figure 5. (a) Melt pools in macroscopic length scale, (b) EBSD image of SLM 316L stainless steel showing elongated grains inside the melt pools at microscopic length scale, (c) SEM image showing existence of a substructure inside the micro grains, (d) SEM image showing the substructure has a cellular morphology with size around 1 µm, (e) the cellular substructure in 420 martensitic stainless steel, (f) nano metric martensite needles inside the cells and across the cells in 420 steel (figures have not been published elsewhere).

http://dx.doi.org/10.5772/intechopen.80468

of stainless steels network of melt pools are created at the macroscopic levels. The size of the melt pools is determined by the line spacing. The directions of melt pools and how they are built can be adjusted according to the laser scanning pattern. Changing or rotating the scanning pattern could generate complex network of the melt pools in stainless steels. **Figure 4** shows different scanning patterns for SLM 316L, CrCoMo dental alloy and SLM 2507.

During the SLM process, upon rapid solidification in the small volume of melt pool various crystallization processes can take place at microscopic level (**Figure 5a**). Inside the melt pools grains are formed as seen in from the EBSD orientation mapping showing elongated grains (**Figure 5b**). At the sub-micron scale and nano levels inside the grains a substructure is seen which is sown in **Figure 5c**. The substructure has cellular morphology with cells around 1 μm (**Figure 5d**). Hierarchy in laser melted 420 martensitic stainless steel is depicted in **Figure 5e** and **f** where cellular structure in micron scale (**Figure 5e**) and colonies of martensitic needles with different orientation in submicron scale (**Figure 5f**) are seen.

Hierarchical microstructure heterogeneities at two length scales macro and micro are present in the laser melted stainless steels. The microstructure heterogeneities can be categorized to grain morphology, grains size and orientation. **Figure 6a** shows existence of different

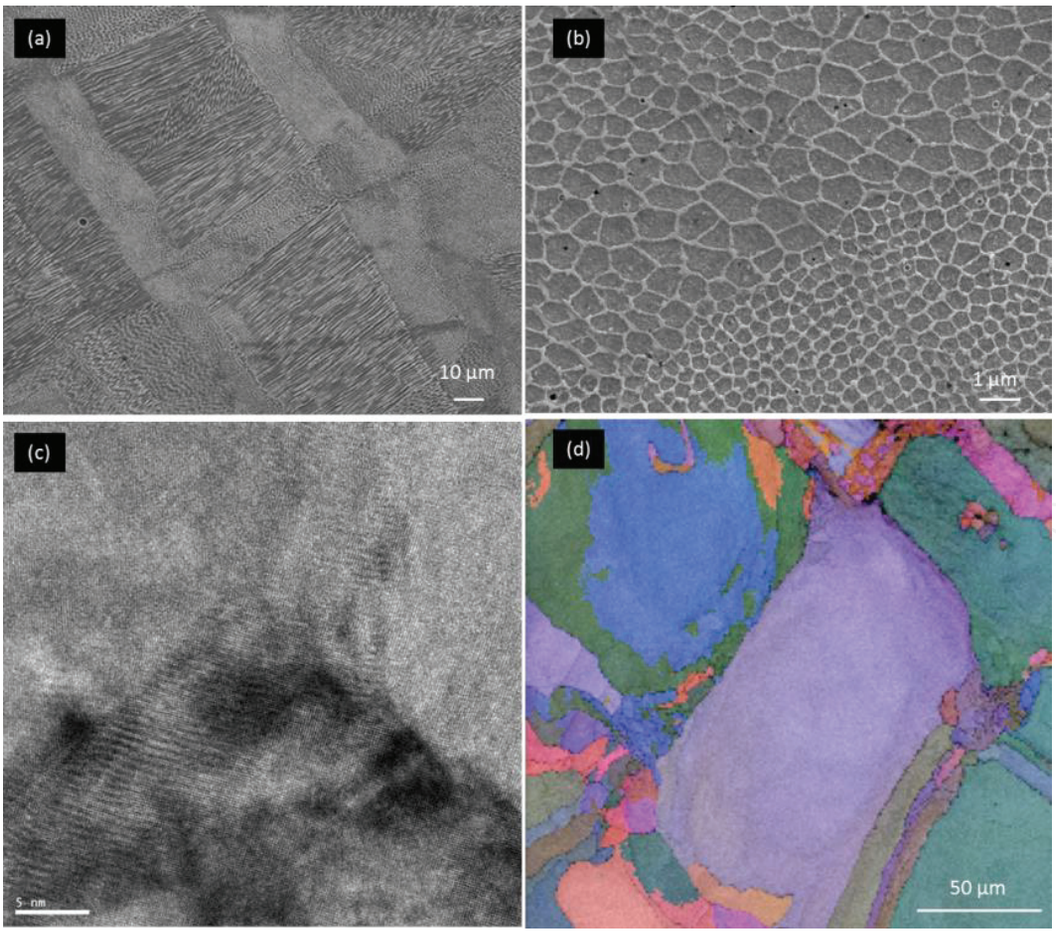

Figure 6. SEM images of SLM 316L showing (a) different grain morphology existing inside the melt pools, (b) cells with different sizes, (c) HRTEM image from SLM 316 L indicating different orientation of subgrains inside bigger grains, (d) EBSD images from SLM 2507 stainless steel confirming existence of smaller grains in between the tesserae and inside each tesserae (figures have not been published elsewhere.).

microstructure patterns, such as hexagonal cells, columnar and band structure. **Figure 6** illustrates these heterogeneities clearly. **Figure 6a** shows existence of different microstructure patterns, such as hexagonal cells, columnar and band structure. In **Figure 6b**, cells with different sizes are seen. As shown by the HRTEM in **Figure 6c**, the cells next to each other coexisting in a bigger grain have different orientations.

EBSD image reveals the existence of different grain size and orientation in duplex 2507 stainless steel processed by laser melting (**Figure 6d**). Morris et al. [29] proved the cellular substructure is in fact subgrains with low angle grain boundaries (LAGBs) that are confined in the bigger grains with high angle grain boundaries. The measured misorientation of two adjacent cells (subgrains) was around two degrees, further supporting their claim.

3. Mechanical properties of stainless steels

3.1. Mechanical performance and microstructural studies of SLM stainless steels at room temperature (25°C)

Stainless steels are primarily utilized because of their corrosion resistance, low cost and room temperature mechanical properties. The properties of stainless steels result from both its chemical composition, microstructure characteristics and its method of manufacture, including processing during fabrication. This section addresses room temperature mechanical properties of stainless steel grades (316L, 2507, 420) manufactured by SLM and a comparison is made with conventional steels. **Figure 7** shows the tensile test curve of SLM 316L at room temperature (a) and the corresponding micrograph of fracture surface (b).

The mechanical properties are listed in **Table 1**. As seen, the SLM 316L shows yield strength of 456 MPa and tensile strength of 700 MPa and microhardness of 325 Hv. These properties are higher than all conventional 300 series steels with yield strength between 240 and 300 MPa, tensile strength between 500 and 650 MPa and microhardness in the range of 140–180 Hv [30]. The ductility of the SLM 316L however is similar to conventional 316L. Despite having a high ductility, one major drawback of conventional 316L stainless steel is its low yield strength (~250–300 MPa) [31]. Many traditional metallurgical routes for strengthening 316L (for example, cold rolling, forging) inevitably results in a severe drop in ductility. To date, despite decades of studies the strategies to achieve both high strength and ductility remain rare. However, the mechanical strength of the SLM 316L is superior without sacrificial loss of ductility. Therefore, the SLM fabrication can overcome the strength–ductility trade-off that exists ubiquitously in pure metals and alloys [29].

The underlying mechanism breaking the strength-ductility trade has been investigated by detailed characterization of SLM 316 stainless steel (**Figure 8**). The SLM 316L possesses hierarchically heterogeneous microstructure with fine micron sized cellular subgrains with one or more orientation confined by macro grains (**Figure 8a**). The subgrains are formed by enrichment of elements such as Cr and Mo investigated by STEM and elemental mapping

http://dx.doi.org/10.5772/intechopen.80468

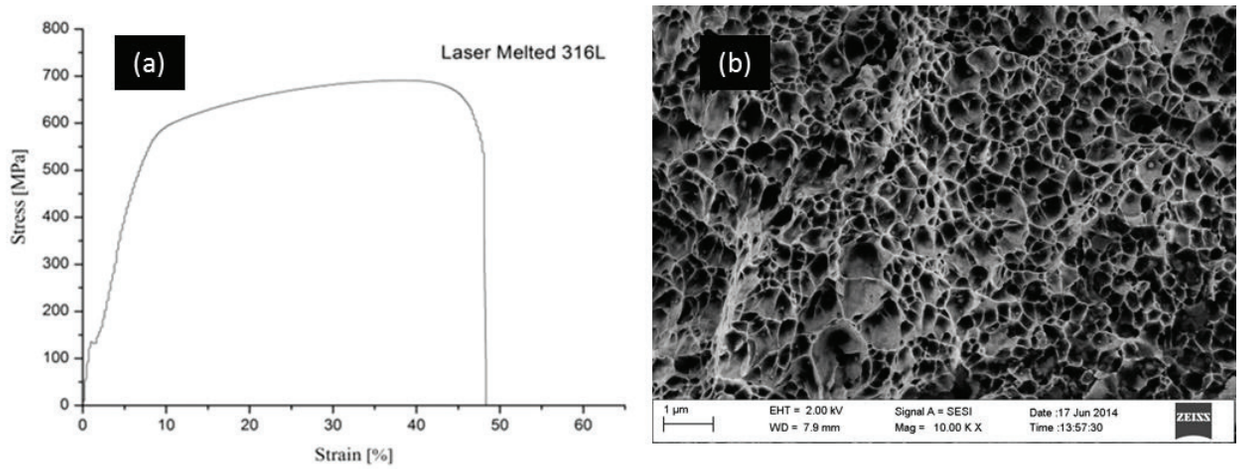

Figure 7. (a) Tensile test curve obtained from SLM 316 L at room temperature, (b) scanning electron micrograph of the fracture surface showing ductile dimples with size less than 1 μm (figures have not been published elsewhere).

Steel Type	Yield strength (MPa)	Tensile strength (MPa)	Elongation (%)	Hardness (Hv)
Austenitic	240-300	500-650	40-45	140-180
Ferritic	270-450	420-750	15-13	250-400
Martensitic	400-800	500-1100	10-15	280-560
Duplex	400-550	700-1000	20-25	270-310
SLM 316L[a]	456	703	45	325

Table 1. Mechanical properties of stainless steel types and comparison with SLM 316 L.

(**Figure 8b**). Movement of Mo with a large atomic radius around 1.99 Å inside the steel matrix generates lots of stress and forms dislocation loops (**Figure 8c**) [17]. Dislocation interactions with each other and with low angle grain boundaries (**Figure 8d** and **e**), formed by the subgrains, increases the mechanical strength whilst presence of slip planes, deformation twins [29] and different subgrain size avoids ductility loss. The superior properties arise from the collective effects of hierarchically heterogeneous microstructures, including solidification cellular structure, LAGBs, and dislocations.

Room temperature mechanical properties of SLM duplex 2507 are listed in **Table 2**. The material exhibits a superior mechanical strength with yield strength of 1200 MPa, tensile strength of 1320 MPa and microhardness of 450 Hv which are almost two times higher than all grades of ferritic and duplex stainless steel reported by AutoCompu [30]. However, the elongation of the studied SLM 2507 is two times lower than conventional duplex steels (10% for SLM 2507 compared to 20–25% for conventional duplex stainless steels).

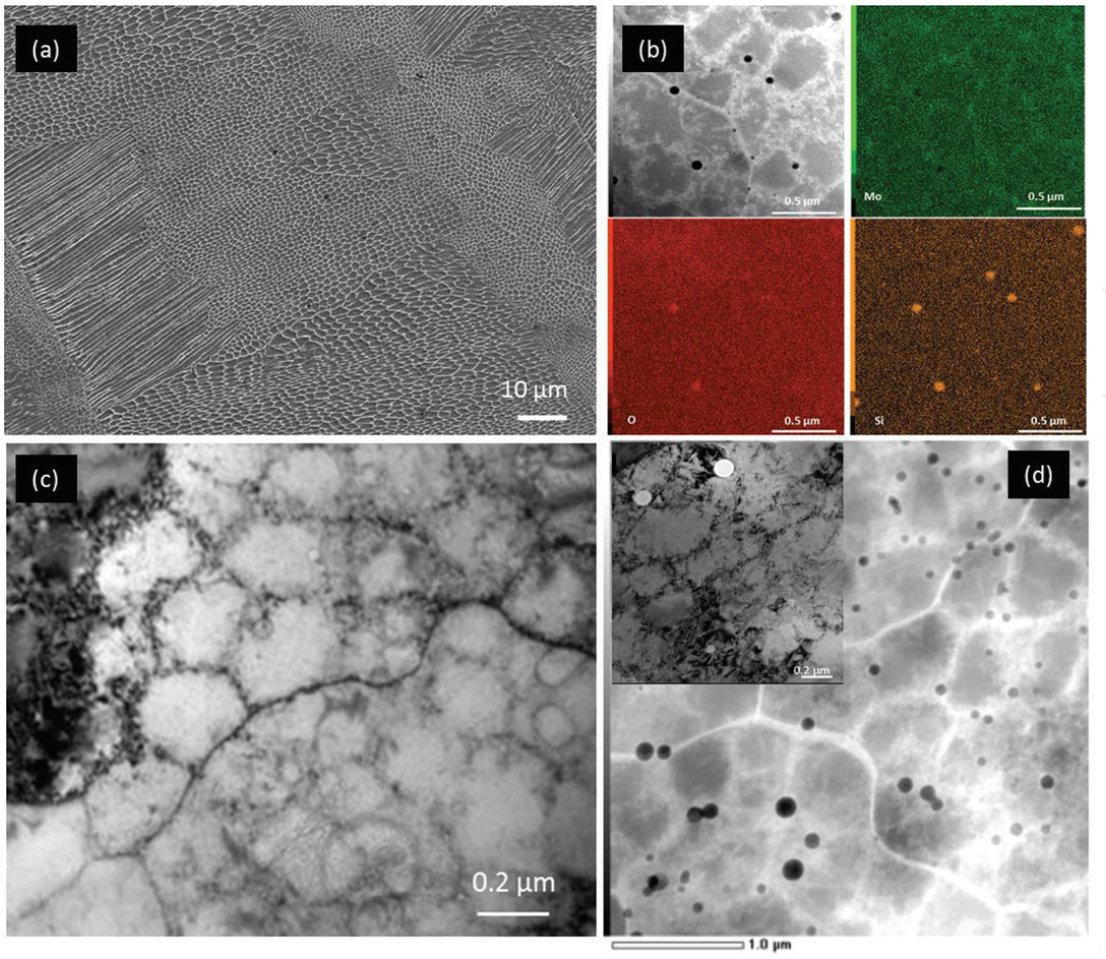

Figure 8. (a) SLM 316L possesses hierarchically heterogeneous microstructure with fine micron sized cellular subgrains with one or more orientation confined by macro grains, (b) STEM and elemental mapping indicating subgrains are formed by enrichment of elements such as Cr and Mo (copyright obtained; *DOI: 10.1039/C4RA16721J*), (c) bright field TEM image showing dislocation loops formed around the cell boundaries (copyright obtained; DOI: 10.1016/j.msea.2014.12.018), (d) oxide nano inclusions strengthening the 316L steel by pinning the dislocation movement as seen from the inset.

Type	Tensile strength (MPa)	Yield strength (MPa)	Microhardness (HV)
SLM Duplex	1321±48	1214±43	450
Duplex SS	600-800	400-550	200-250
Ferritic SS	400-600	250-400	135-175

Table 2. Comparison of room temperature mechanical properties of SLM duplex with conventional duplex and ferritic stainless steel.

The reason behind superior mechanical strength is combination of macro mosaic texture containing grains shown by EBSD image (**Figure 9a** and **b**) very dense 3D network of dislocation forming loops with diameter of 200 nm (**Figure 9c** and **d**), nitrogen enriched zones and formation of hard and brittle nitrides (**Figure 9e** and **f**).

http://dx.doi.org/10.5772/intechopen.80468

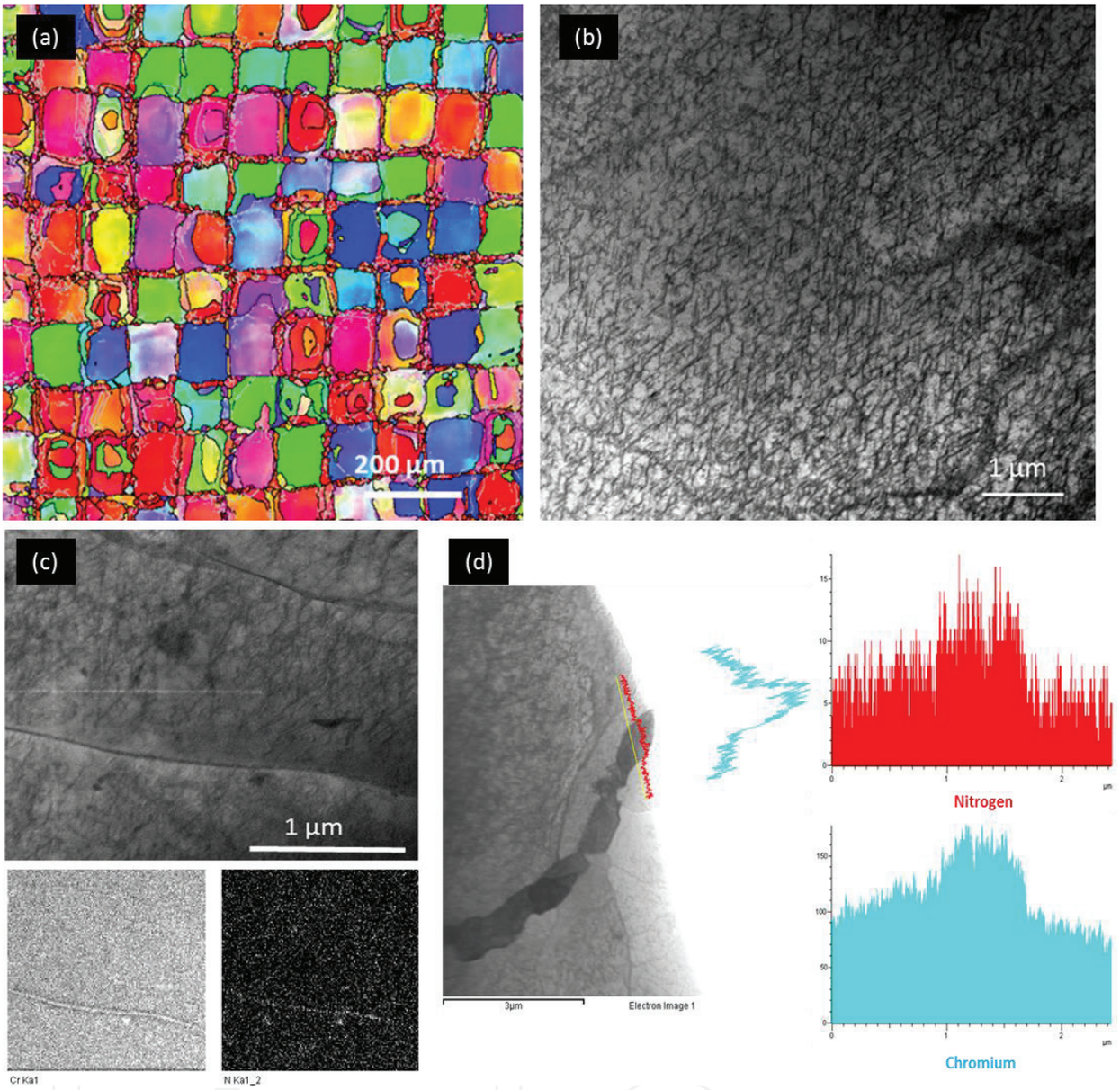

Figure 9. EBSD image of (a) top view of SLM duplex 2507 stainless steel showing a mosaic texture in which each tesserae contains grains, (b) dense 3D network of dislocations forming loops approximately 200 nm, (c) TEM mapping showing nitrogen enriched zones, (d) TEM line scanning revealing nitrides (copyrights obtained; DOI: 10.1016/j.msea.2016.04.027).

SLM fabricated martensitic stainless steel, grade 420, demonstrated hard material with microhardness of 650 Hv and excellent mechanical strength (1800 MPa tensile strength and 800 MPa yield strength) with low toughness i.e., 4–5% of elongation. The strength and microhardness of 420 grade processed by SLM exceeds that of tools steels reported [32, 33]. The superior mechanical strength can be explained by presence of fine cellular structure with submicron martensitic needles. The size of the martensite needles in SLM fabricated martensitic stainless steel, grade 420 is finer than martensitic needles formed by quench and partitioning reported in literature [34, 35]. The colonies of fine cells and submicron martensitic needles can effectively promote the mechanical strength of the SLM 420 material. **Table 3** compares the mechanical properties of SLM 420 with conventional processed AISI 420 stainless steel.

3.2. Mechanical performance and microstructural studies at intermediate temperatures (250–800°C)

The structure materials for in-vessel components of the international thermonuclear experimental reactor (ITER) will require the material to withstand temperature of the working environment (estimated around 200–250°C). 316L stainless steel has been selected as one candidate due to its combination of good mechanical properties, excellent corrosion resistance and good machinability [36, 37]. Challenging issue of the ITER in-vessel components is their geometrical complexity containing inner structure details, like piping systems. These components are difficult to build, costly and sometimes even impossible to build by any conventional manufacturing process. 316L manufactured by SLM shows to be promising for building complex components with enhanced properties. Zhong et al. [38] studied the mechanical properties of SLM 316L at 250°C and made a comparison with the required properties suitable for ITER. **Table 4** shows the mechanical properties of SLM 316L, HIP 316L and the properties required for ITER. As seen, the mechanical properties of the SLM 316L at room temperature and 250°C are higher than the strength requirement for an ITER component. This study successfully confirmed that the SLM was a suitable technique for building complex components with enhanced properties required for ITER application. Well-arranged cellular subgrains strengthen SLM 316L by dislocation pinning effect following Hall-Petch rule and give rise to higher strength and lower ductility than EBM 316L. However larger columnar grains and irregular subgrains in EBM 316L results in higher ductility and higher toughness than SLM 316L [38].

Industrial demands for stainless steel components and parts to be used at higher service temperatures have attracted attentions towards using stainless steels for high temperature applications. Thus, today, steels such as martensitic grade 403 steel is used in gas turbines at 550–600°C [39] and A286 austenitic stainless steel is used in jet engines at 700°C [40]. The need

Type of material	Tensile strength (Mpa)	Yield strength (Mpa)	Elongation (%)	Microhardness (HV)
SLM 420	1800 MPa	800 Mpa	5%	650 HV
Annealed cold drawn AIS 420 [32]	800 MPa	700 Mpa	6-7%	-----

Table 3. Table comparing SLM 420 stainless steel with the mechanical properties of conventionally cold drawn 420 stainless steel.

316L type	Yield Strength (MPa)	Tensile strength (MPa)	Total Elongation (%)
SLM at RT	487 ± 3	594 ± 4	49 ± 4
SLM at 250 °C	376 ± 3	461 ± 3	31 ± 4
HIP at RT/200 °C	220/160	570/450	54/42
Criteria RT/ET	220/135	525/415	45/-
EBM at RT	253 ± 3	509 ± 5	59
EBM at 250 °C	152 ± 3	386 ± 3	46 ± 3

Table 4. Mechanical properties of SLM 316L and EBM 316L at room and 250°C temperature and properties criteria for ITER application.

for a low cost, easy to machine and widely used stainless steel such as 316L has been realized. The 316L is typically utilized at service temperatures up to 500°C [41, 42] whereas above 500°C, the steel undergoes composition and microstructure changes such as precipitation of unwanted phases and grain coarsening that degrades its performance.

Figure 10a shows the mechanical performance of SLM 316L at 800°C. The material withstands tensile stress of 400 MPa before failure compared to 180 MPa for conventional 316L and 304 stainless steels. The tensile test curve is divided into three regions. In the first region the stress reaches a plateau of 100 MPa while simultaneously stretching and elongating to 10%. The reason for this the structural hierarchy presented in the steel microstructure after SLM which remains despite being heated to 800°C. The hierarchy can be verified from the EBSD figures where the melt pools with width of 100 μm are seen and inside the melt pools array of elongated grains are observed which themselves contain smaller subgrains (**Figure 10b** and **c**). In the second region, strain strengthening effect occurs, i.e. after the yield point elongation deformation proceeds uniformly. These phenomena are due to the fine micron sized

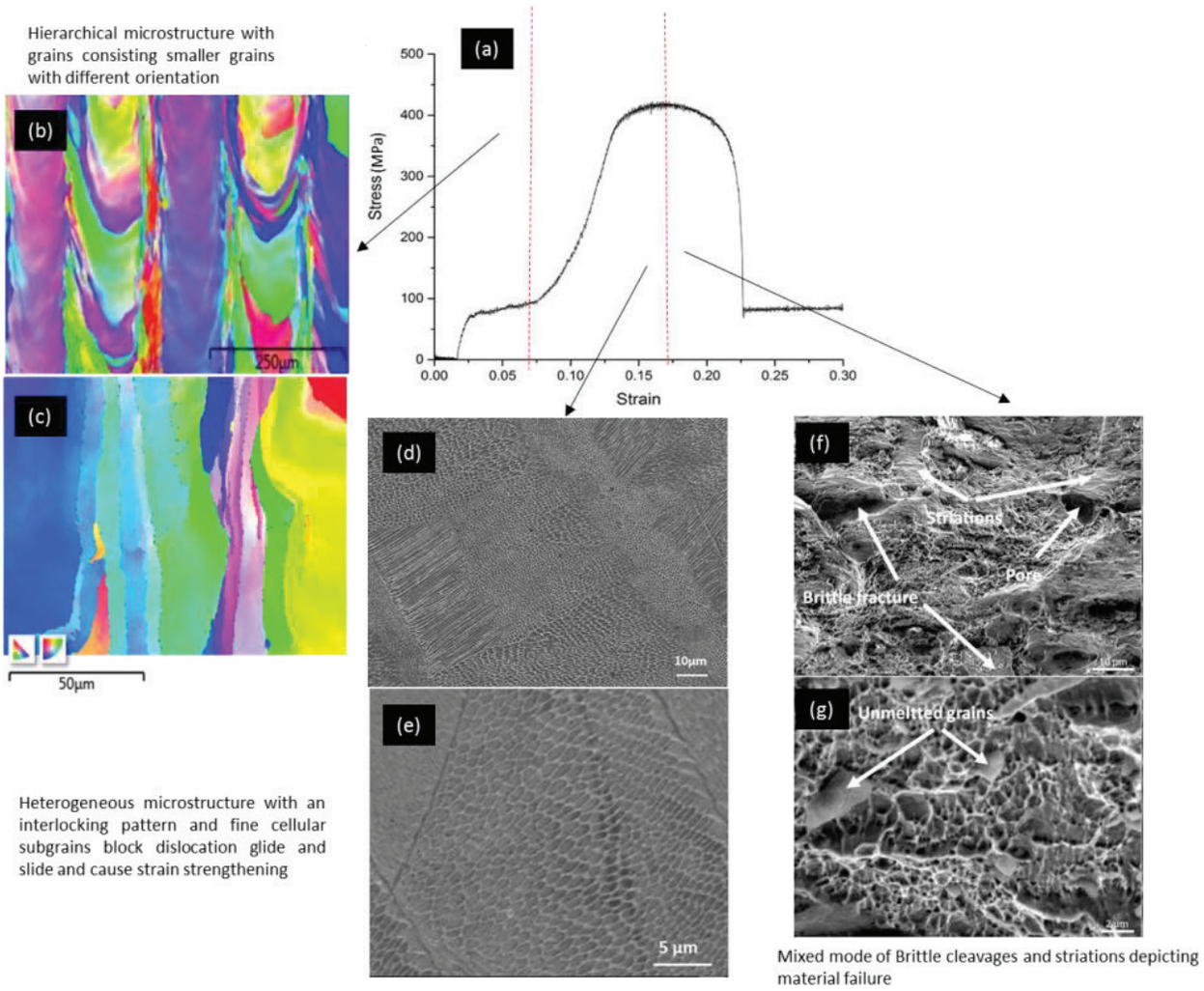

Figure 10. (a) Tensile test curve of SLM 316 L obtained at 800°C and divided into three regions, (b and c) in the first region the hierarchy verified from the EBSD figures cause strengthening, (d and e) fine micron sized subgrains interacting with dislocation movement, (f and g) fracture analysis showing a dual ductile-brittle fracture mode with striations, cup and cone dimples and brittle cleavages (copyrights obtained; DOI: 10.1016/j.matdes.2017.08.072).

subgrains (see **Figure 10d** and **e**) inhibiting dislocation movement. These phenomena are typical in materials with low stacking fault energies such as austenitic stainless steels. In the third region threshold value of the material is reached after 400 MPa stress and the materials fails in a dual ductile-brittle mode. **Figure 10f** and **g**) shows striations, cup and cone dimples and brittle cleavages confirming a dual failure mode.

3.3. Mechanical performance and microstructural studies of SLM stainless steels at high temperatures (>800°C)

The microstructure of a polycrystalline material is a key parameter in determining a wide range of its properties including mechanical strength, toughness, electrical conductivity and magnetic susceptibility [43, 44]. One important aspect of microstructure is the size of the grains and its influence on the properties. Thus, to design the grain size and restrict grain growth, microstructural engineering has become of fundamental importance [45]. High temperature applications are critically influenced by grain growth, precipitation and phase changes. Biggest issue which is very common and probable in materials exposed at high temperatures is the abnormal grain growth, where one or more grains will grow abnormally in the microstructure. The presence of abnormally large grains is detrimental to the mechanical properties of polycrystalline structures [46]. Mechanical properties of SLM 316L at 1100 and 1200°C is listed in **Table 5** and compared to conventional 316L materials at the same temperature [47].

The Superior, 10 times higher, mechanical strength of 300 and 150 MPa of 316L SLM (for temperatures 1100 and 1200°C respectively) compared to 35–40 and 20 MPa, points out that the rapid grain growth and loss of strength has been avoided. The growth mechanism involved in this case is "subgrain controlled mechanism" shown by the schematic in **Figure 11a**. In step one, the cellular subgrains inside and confined by the macro grains (shown by the hexagon) are seen. During heating at temperatures up to 1100°C (step 2) the subgrain boundaries merge with adjacent subgrains and form larger subgrains while still being confined by the larger macro grains. In step three, upon heating to temperatures ≥1200°C the cellular subgrains have disappeared and new subgrains with irregular shapes have formed which are bigger than 1 μm and are still confined inside the macro grains. This continues until at very high temperatures (>1200°C) the subgrains have grown into the size of the macro grain and from this point on the macro grains will start to grow and abnormal grain growth can possibly occur. SEM microscopy observation shows the clear tendency of subgrains merging into bigger

Type	Grain size (μm)	Tensile strength (MPa)	Elongation (%)
SLM-1100°C	5-16 μm	300 MPa	15-18%
SLM-1200°C	32 μm	150 MPa	20%
Casted-1100°C	50 μm	35-40 MPa	40%
Casted-1200°C	80 μm	20 MPa	45%

Table 5. Mechanical properties of SLM 316L at 1100 and 1200°C and comparison to conventional 316L materials at the same temperature.

http://dx.doi.org/10.5772/intechopen.80468

subgrains as seen in **Figure 11b** and **c**. The white dashed areas show how the 1 μm-sized cells merge and become a bigger subgrain (approx. 2–5 μm) and the black line marks the boundary of the initial macro sized grain (approx. 10–20 μm) containing the 1 μm subgrains. By applying higher temperature (1200°C), it appears that the subgrains have disappeared and the irregular macro sized grains have remained (see **Figure 11d** and **e**).

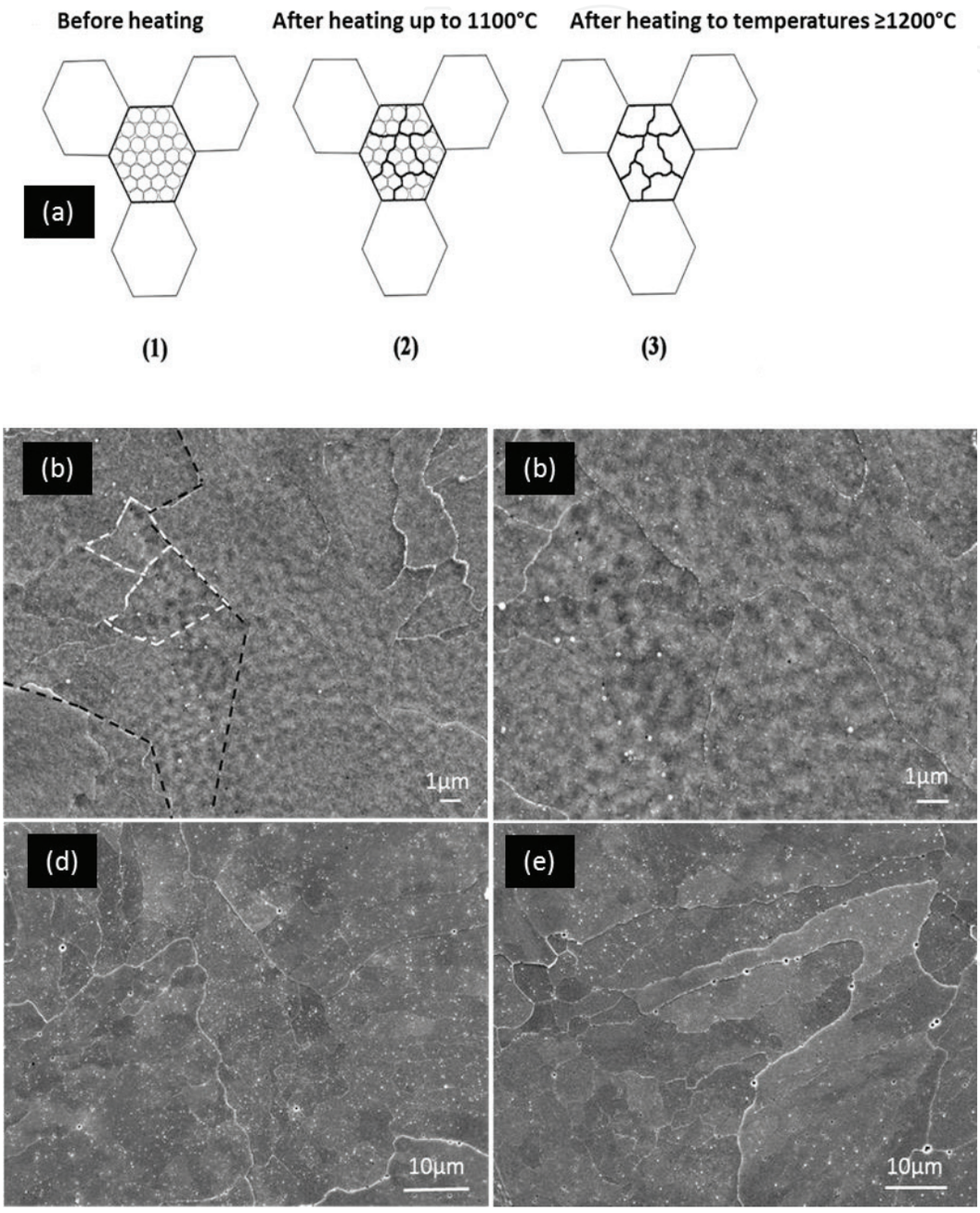

Figure 11. (a) Schematic of the grain growth mechanism in SLM 316L showing three stages before heating, after heating to temperatures up to 1000°C and after heating to temperatures higher than 1200°C, (b and c) SEM microscopy observation shows the clear tendency of subgrains merging into bigger subgrains upon heating to temperature as high 1100°C. The white dashed areas show how the 1 μm-sized cells merge and become a bigger subgrain (approx. 2–5 μm) and the black line marks the boundary of the initial macro sized grain (approx. 10–20 μm) containing the 1 μm subgrains, (d and e) the subgrains have disappeared and the irregular macro sized grains have remained (copyrights obtained; DOI: 10.1098/rsos.172394).

High temperature mechanical properties of SLM 2507 duplex was assessed at 1200°C. The tensile test curve is seen in **Figure 12a**. Comparison with conventional duplex material made in **Table 6** shows significantly higher strength of SLM 2507 material with tensile strength of 200 MPa. The high strength is due to the fine microstructure consisting of columnar grains of austenite (100 μm in length and 2–4 μm in width) and ferrite grains in between them (**Figure 12b**). The interlocking network strengthens and toughens the material at the same time, showing 30% elongation before failure. The ductile failure mode is confirmed by the cup and cone dimples seen in **Figure 12c** and **d**.

In another study the SLM duplex 2507 was first heat treated to 1200°C in a tube furnace with cooling rate 300°C/hr thereafter mechanical properties of the material was measured at 1200°C. The mechanical strength is around 400 MPa (**Figure 13a**) which is two times higher than one reported in **Figure 12**. Intermetallic phases such as sigma precipitate due to enrichment of Mo and Cr in the matrix of stainless steel (**Figure 13b** and **c**). Due to non-equilibrium nature of SLM 2507 and the high activation energy of Mo and Cr for diffusion, upon heating the material to high temperatures such as 1200°C the diffusion barrier of Mo is met and activation energy for the diffusion is provided thus phase changes and sigma precipitation can occur upon cooling.

Fast cooling rates during heat treatment can influence the formation of intermetallic sigma phase. Studies carried out [48] and shown by TTT diagrams indicate cooling rates (higher

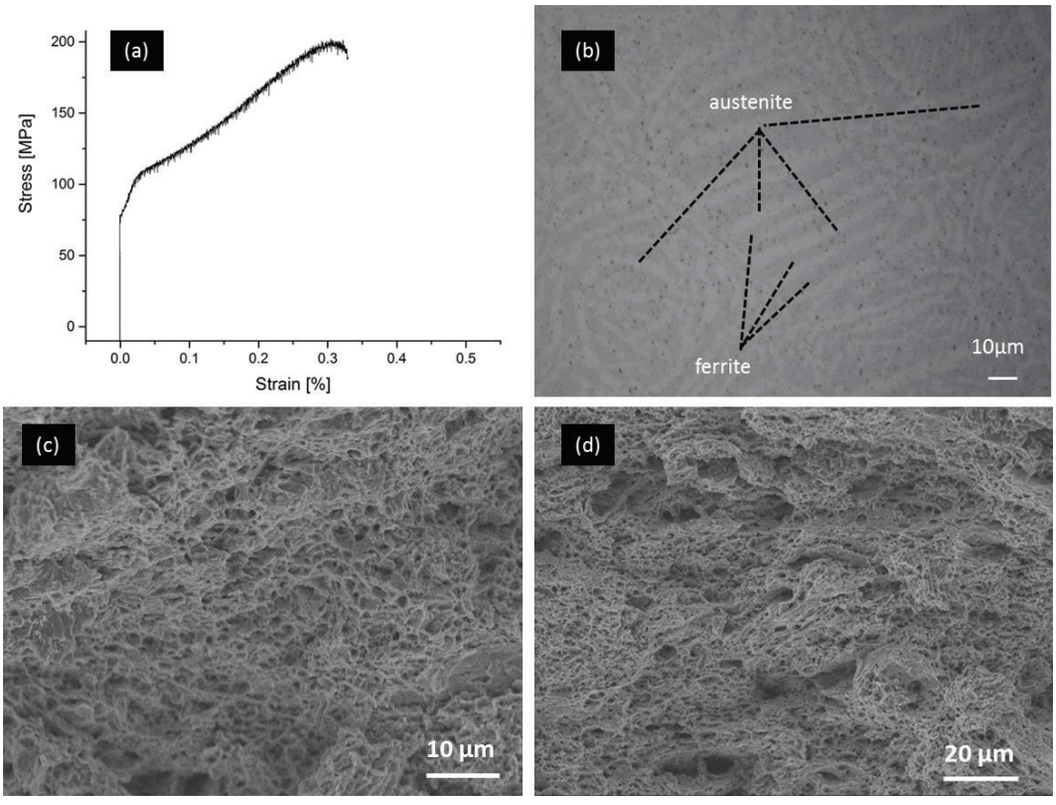

Figure 12. (a) Tensile test curve of SLM 2507 obtained at 1200°C, (b) fine microstructure consisting of columnar grains of austenite (100 μm in length and 2–4 μm in width) and ferrite grains in between them, (c) fracture analysis showing ductile failure mode confirmed by the cup and cone dimples (figures have been used in paper submitted to Journal of Alloys and Compounds on 20/06/2018.).

http://dx.doi.org/10.5772/intechopen.80468

Tensile test at 1200 °C	Tensile strength (MPa)	Elongation (%)
SLM duplex 2507 (without sigma precipitates)	200 MPa	30%
Conventional duplex	19 MPa	----

Table 6. Mechanical properties of duplex stainless steel obtained at 1200°C.

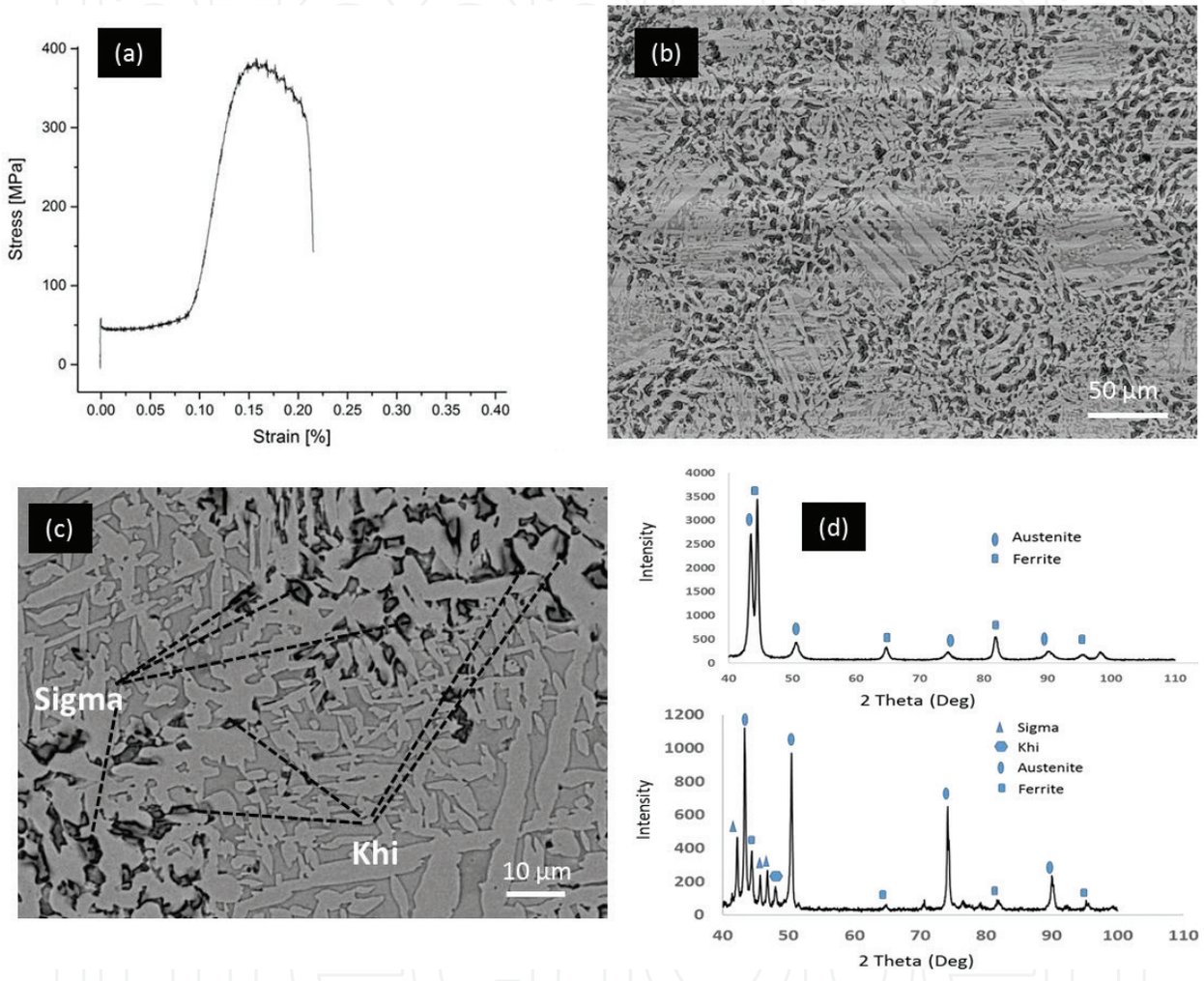

Figure 13. (a) Tensile test curve of heat treated SLM 2507 obtained at 1200°C, (b and c) intermetallic sigma and Khi precipitates, (d) XRD pattern of SLM 2507 with intermetallic and without intermetallic formation (figures have been used in paper submitted to Journal of Alloys and Compounds on 20/06/2018).

than 250°C/hr) can completely avoid sigma precipitation. The test instrument for the high temperature mechanical testing is Gleeble[3800]. The cooling rate in vacuum in the Gleeble chamber is approximately 200°C/s which is much higher than 250°C/hr and thus sigma can totally be avoided. Therefore, the material heat treated at slow cooling rates precipitates sigma phase, which are strong and brittle phase precipitates (see **Figure 13b** and **c**). Formation of sigma phase strengthens the material and causes higher strength as compared to material with no sigma phase (see XRD patterns in **Figure 13d**).

4. Conclusions

Tailoring microstructure, tuning the chemistry, adjusting phase composition and introducing dense 3D network of dislocations through fast cooling processes such as selective laser melting can tailor and develop stainless steels with high performance for extreme conditions, such as elevated temperatures. The very fine cellular sub-grains and Mo enrichment at the cell boundaries can enable the material to withstand more stress and higher temperatures. The non-equilibrium phase composition and phase transformations obtained after laser melting can strengthen the material via formation of coarser martensitic needles (in 420 stainless steel) and intermetallic phases (in 2507 duplex stainless steel) upon post heat treatment.

Acknowledgements

The authors would like to thank the funding support from the Carl Tryggers Foundation (grant no. CTS 16:6) and the Swedish Foundation for Strategic Research (SSF) for an infrastructure fellowship grant (RIF14-0083).

Conflict of interest

The authors declare that they have no conflict of interests.

Notes/Thanks/Other declarations

The authors would like to thank Emil Hedin, Valeri Ivanov and Daniel Zapata for sample preparations and helping out with the characterizations.

Author details

Kamran Saeidi* and Farid Akhtar

*Address all correspondence to: kamran.saeidi@ltu.se

Department of Mathematics and Engineering Sciences, Division of Engineering Materials, Luleå University of Technology, Luleå, Sweden

References

[1] Gibson I, Rosen DW, Stucker B. Additive Manufacturing Technologies. NewYork, USA: Springer; 2010

[2] Feygin M, Pak SS. Laminated Object Manufacturing Apparatus and Method. Google Patents; 1999

[3] Zein I, Hutmacher DW, Tan KC, Teoh SH. Fused deposition modeling of novel scaffold architectures for tissue engineering applications. Biomaterials. 2002;**23**(4):1169-1185

[4] Jacobs PF. Rapid Prototyping & Manufacturing: Fundamentals of Stereolithography. Society of Manufacturing Engineers. NewYork, USA: McGraw-Hill; 1992

[5] Ibrahim D, Tiago LB, Heitz C, De Oliveira MG, De Oliveira HW. Dimensional error of selective laser sintering, three-dimensional printing and PolyJet™ models in the reproduction of mandibular anatomy. Journal of Cranio-Maxillofacial Surgery. 2009; **37**(3):167-173

[6] Stotko CM. Laser sintering: Layer by layer. Nature Photonics. 2009;**3**(5):265-266

[7] Kruth J-P, Froyen L, Van Vaerenbergh J, Mercelis P, Rombouts M, Lauwers B. Selective laser melting of iron-based powder. Journal of Materials Processing Technology. 2004; **149**(1):616-622

[8] Gu D. Laser Additive Manufacturing of High-Performance Materials. Heidelberg, Germany: Springer; 2015

[9] Cormier D, Harrysson O, West H. Characterization of H13 steel produced via electron beam melting. Rapid Prototyping Journal. 2004;**10**(1):35-41

[10] Heinl P, Muller L, Korner C, Singer RF, Muller FA. Cellular Ti–6Al–4V structures with interconnected macro porosity for bone implants fabricated by selective electron beam melting. Acta Biomaterialia. 2008;**4**(5):1536-1544

[11] Harrysson OL, Kansyzoglu O, Marcellin-little DJ, Cormier DR, West HA. Direct metal fabrication of titanium implants with tailored materials and mechanical properties using electron beam melting technology. Materials Science and Engineering C. 2008; **28**(3):366-373

[12] Atwood C. Laser Engineered Net Shaping (LENS (TM)): A Tool for Direct Fabrication of Metal Parts. Albuquerque, NM/Livermore, CA: Sandia National Laboratories; 1998

[13] Utela B, Storti D, Anderson R, Ganter M. A review of process development steps for new material systems in three dimensional printing (3DP). Journal of Manufacturing Processes. 2008;**10**(2):96-104

[14] Saeidi K. Stainless steels fabricated by laser melting: Scaled down structural hierarchies and microstructural heterogeneities [thesis]. Stockholm University, Department of Materials and Environmental Chemistry; 2016

[15] Beng CH. Selective laser sintering of a stainless steel powder [thesis]. University of Leeds. Leeds, England: School of Mechanical Engineering; 2003

[16] Miranda G, Faria S, Bartolomeu F, Pinto E, Madeira S, Mateus A. Predictive models for physical and mechaical properties of 316L stainless steel produced by selective laser melting. Materials Science Engineering A. 2016;**657**:43-56

[17] Sun Z, Tan X, Tor SB, Yeong WY. Selective laser melting of stainless steel 316L with low porosity and high build rates. Materials and Design. 2016;**104**:197-204

[18] Saeidi K, Gao X, Zhong Y, Shen J. Hardened austenite steel with columnar sub-grain structure formed by laser melting. Journal of Materials Science Engineering A. 2015; **625**:221-229

[19] Wang H, Sweikart MA, Turner JA. Stainless steel as bipolar plate material for polymer electrolyte membrane fuel cells. Journal of Power Sources. 2003;**115**:243-251

[20] Dewidar MM, Khalil KA, Lim J. Processing and mechanical properties of porous 316L stainless steel for biomedical applications. Transactions of Nonferrous Metals Society of China. 2007;**17**:468-473

[21] Xu FL, Duan JZ, Lin CG, Hou B. Influence of marine aerobic biofilms on corrosion of 316L stainless steel. Journal of Iron and Steel Research, International. 2015;**22**:715-720

[22] Kastelic J, Galeski A, Baer E. The multicomposite structure of tendon. Connective Tissue Research. 1978;**6**:11-23

[23] Weiss PS. Hierarchical assembly. ACS Nano. 2008;**2**:1085-1087

[24] National Research Council and others. Hierarchical Structures in Biology as a Guide for New Materials Technology. Washington, DC: National Academy Press; 1994. p. 464

[25] Vogel F, Wanderka N, Balogh Z, Ibrahim M, Stender P, Schmitz G, Banhart J. Mapping the evolution of hierarchical microstructures in a Ni-based super alloy. Nature Communications. 2013;**4**:1-7

[26] Song JE. Hierarchical multisacle modeling of Ni-base super alloys [Master of Science thesis]. Georgia Institute of Technology. Atlanta, USA: School of Mechanical Engineering; 2010

[27] Kurella AK. Laser induced hierarchical coatings on titanium alloy [Doctor of Philosophy thesis]. Knoxville: University of Tennessee; 2009

[28] Liu G, Dingdong F, Li J, Chen K, He G, Yang Z, Guo S. Combustion synthesis of W–Cr alloys with hierarchical microstructure and improved hardness. Materials Letters. 2016; **166**:43-45

[29] Morris Wang Y, Voisin T, McKeown JT, Ye J, Calta NP, Li Z, et al. Additively manufactured hierarchical stainless steels with high strength and ductility, Nature Materials. 2018;**17**:63-71

[30] Seritova M. Handbook of Stainless Steel. Espoo, Finland: Autokumpu; 2103

[31] Yan FK, Liu GZ, Tao NR, Lu K. Strength and ductility of 316L austenitic stainless steel strengthened by nano-scale twin bundles. Acta Materialia. 2012;**60**:1059-1071

[32] Chen H, Gu D, Dai D, Ma C, Xia M. Microstructure and composition homogeneity, tensile property, and underlying thermal physical mechanism of selective laser melting tool steel parts. Materials Science and Engineering: A. 2017;**682**:279-289

[33] Brnic J, Turkalj G, Canadija M, Lanc D, Krscanski S. Martensitic stainless steel AISI 420—Mechanical properties creep and fracture toughness. Mechanics of Time-Dependent Materials. 2011;**15**:341-352

[34] Kitahara H, Ueji R, Tsuji N, Minamino Y. Crystallographic features of lath martensite in low-carbon steel. Acta Materialia. 2006;**54**:1279-1288

[35] Lu SY, Yao KF, Chen YB, Wang MH, Chen N, Ge XY. Effect of quenching and partitioning on the microstructure evolution and electrochemical properties of a martensitic stainless steel. Corrosion Science. 2016;**103**:95-104

[36] Kalinin G, Barabash V, Cardella A, Dietz J, Ioki K, Matera R. Assessment and selection of materials for ITER in-vessel components. Journal of Nuclear Materials. 2000;**283**:10-19

[37] Tavassoli AA. Assessment of austenitic stainless steels. Fusion Engineering and Design. 1995;**29**:371-390

[38] Zhong Y, Rännar LK, Wikman S, Koptyug A, Liu L, Cui D, Shen Z. Additive manufacturing of ITER first wall panel parts by two approaches: Selective laser melting and electron beam melting. Fusion Engineering and Design. 2017;**116**:24-33

[39] Muktinutalapati NR. Materials for gas turbines—An overview. In: Benini E, editor. Advances in Gas Turbine Technology. InTech; 2011. pp. 293-314

[40] De CH, Luppo MI, Raffaeli H, Di Gaetano J, Gribaudo LM, Ovejero-García J. Creep behavior of an A286 type stainless steel. Materials Characterization. 2005;**55**:97-105

[41] Hoke JH. Mechanical properties of stainless steels at elevated temperatures. Handbook of Stainless Steels. NewYork, USA: MacGraw-Hill; 1977

[42] Davies CM. Predicting creep crack initiation in austenitic and ferritic steels using the creep toughness parameter and time-dependent failure assessment diagram. Fatigue and Fracture of Engineering Materials and Structures. 2009;**32**(10):820-836

[43] Li JCM. Microstructure and Properties of Materials. Vol. 1. Singapore: World Scientific Publishing; 1996. ISBN: 978-981-02-2403-5

[44] Penn SJ, Alford MN, Templeton A, Wang X, Xu M, Reece M, Scharp K. Effect of porosity and grain size on the microwave dielectric properties of sintered alumina. Journal of American Ceramic Society. 1997;**80**:1885-1888

[45] Davidson KP, Singamneni S. Magnetic characterization of selective laser melted SAF 2507 duplex stainless steel. Journal of Metals. 2017;**69**:569-574

[46] Dennis J, Bate PS, Humphreys JF. Abnormal grain growth in metals. Material Science Forum. 2007;**558-559**:717-722

[47] Saeidi K, Akhtar F. Sub-grain controlled grain growth in laser melted 316L promoting strength at high temperatures. Royal Society Open Science. 2018;**5**:172394

[48] Padilha AF, Aguiar DJM, Plaut RL. Duplex stainless steels: A dozen of significant phase transformations. Defect Diffusion Forum. 2012;**322**:163-174

IntechOpen